京都大学防災研究所年報 第 61 号 B 平成 30 年
DPRI Annuals, No. 61 B, 2018

Estimation of The Strong Motions at Mashiki Town, Kumamoto, During The 2016 Kumamoto Earthquake, Based on Microtremor Horizontal-to-Vertical Spectral Ratios

Jikai SUN, Hiroshi KAWASE and Fumiaki NAGASHIMA

Abstract

We performed microtremor survey in Mashiki Town, Kumamoto, Japan by the single station method after the 2016 Kumamoto earthquake. We obtained microtremor data at 62 sites in the area of 1200m by 1000m. Then we calculated Microtremor Horizontal-to-Vertical Spectral Ratio (MHVR) of every site and gained 48 reliable MHVR curves. After deciding peak frequency on every MHVR curve, we made a fundamental peak frequency map of Mashiki Town. After that, we transformed MHVR to pEHVR by the MHVR-to-EHVR method. We calculated EHVR of two strong motion stations which are located at Mashiki Town, then we compared them with pEHVRs of the nearest microtremor sites. We found that pEHVRs are closer to EHVRs than MHVRs. Then, we identified one-dimensional (1D) S-wave velocity structues of Mashiki Town, by using the Hybrid Heuristic Searching method. Next, we analyzed 1D dynamic soil responses of all the sites by the nonlinear equivalent linear method. We analyzed both linear and nonlinear cases for comparison and we estimated peak ground velocity (PGV) and peak ground acceleration (PGA) of all the sites. We found PGVs showed stable while PGA were significantly different from each site.

Keywords: MHVR, pEHVR, velocity structure, equivalent linear analysis method

1. Introduction

A sequence of two strike-slip earthquakes occurred in the intraplate region of Kyushu Island, Japan (Goda et al., 2016). At 21:26:34 on April 14th, 2016 (JST, UT+9h), the M_{JMA} 6.4 (the Japan Meteorological Agency magnitude) foreshock occurred on the Hinagu fault, and the focal depth was 11km. 28 hours later, the mainshock (M_{JMA} 7.3) hit nearly the same location along the Futagawa fault (northeast of the Hinagu fault) at 01:25:05 on April 16th, 2016 (JST), and its focal depth was 12km(Kawase et al., 2017; Yamada et al., 2017; Fukuyama & Suzuki, 2016). The foreshock caused the major earthquake damage in Mashiki Town near the epicenter. the mainshock caused more serious and wider earthquake damage near Futagawa fault, such as Mashiki Town, Nishihara Village and South Aso Village. In Mashiki Town, the JMA seismic intensity was 7 during both the foreshock and mainshock (Goda et al., 2016). Seven people were killed in mashiki town during the foreshock, and twelve people lost their lives in the mainshock because of building collapse (Yamada et al., 2017).

The heavily damaged areas of wooden buildings spread in a narrow belt (about 50 km long) along the Futagawa and Hinagu fault zones. Approximately 30% of the heavily damaged buildings in the Kumamoto Prefecture were concentrated in the Mashiki Town (Goto et al., 2017). More than 80% of wooden building damage was reported in several 100m survey grids (National Institute for Land and Infrastructure Management (NILIM), 2016; Kawase et al., 2017). The damage area of Mashiki Town formed a narrow band between the NO.28 local road and the Akizu river from east to west. In the report of NILIM, they also mentioned no significant correlations between the damaged area and the wooden buildings ages, because

some wooden houses which were respected to the new construction code were seriously damaged (Goto et al., 2017; Yamada et al., 2017). However, it is difficult for researchers to distinguish damage buildings caused in foreshock or in mainshock accurately, as it is only 28 hours between two strong shocks.

Fortunately, there are two strong motion observation stations in Mashiki Town. One is the KiK-net station, number is KMMH16, which is located at the north boundary of Mashiki Town. Another is set by the Instrumental Intensity Seismometer (IIS) of Kumamoto Prefecture, we describe this site as KMMP58, which is located on the first floor of the Mashiki Town Hull (a 3 floor RC building). we obtained earthquake waves of these two events during the mainshock at KMMH16, the peak ground acceleration (PGA) was 1160gal in east-west (EW) direction, and 652gal in north-south (NS) direction. At KMMP58, the EW PGA was 825.402gal and the NS PGA was 756.996gal. The PGAs are different but the distance between KMMH16 and KMMP58 is only about 680m, we want to know whether the subsurface structures affected PGA in Mashiki town or not. Some researchers mentioned that the soil nonlinearity played an important role to cause the difference of ground motions (Goto et al., 2017).

According to damage survey report of NILIM, average damage index around KMMH16 was nearly zero, while the damage index around KMMP58 was about 40%, the damage distribution in Mashiki town indicated really spatial phenomenon. Spatial differences of damage distribution have been observed in other historical earthquakes, they were associated with local ground motions. During the 1995 Kobe earthquake, the damage distribution formed a belt along the strike of the Rokko geological fault (Kawase, 1996). Kawase (1996) conducted to explain damage belt by using ground motion simulation. We consider using the similar method to estimate building damage index and simulate ground motions in Mashiki Town.

To estimate building damage index, we need to simulate strong ground motion below every building. To simulate strong ground motions in Mashiki town, at first, we need to identify S-wave velocity structure beneath Mashiki town. Kawase et al. (2011) and nagashima et al. (2014) have proposed the method to identify S-wave velocity structure based on Earthquake Horizontal-to-Vertical Spectral ratio (EHVR). However, there're only two strong ground motion observation stations, they are not enough to get the accurate subsurface structures. Kawase et al. (2018) found the method to derive the EHVR from the Microtremor HVR (MHVR), because to get enough MHVRs are easier than getting EHVR. Hence, we observed microtremors in Mashiki town and identified the subsurface structures using pseudo EHVR converted from MHVR. Then we estimated the ground motions during mainshock and compared to the observed damage distribution.

2. Microtremor Observation and MHVR Analysis

Site effects plays an important role in characterizing seismic ground motions because they may strongly amplify seismic motions before reaching the surface of the ground or the basement of artificial structures. There are many ways to estimate the site effects. One simple way is to characterize the site effects by soil-type classification, but such estimation has some problems. Aki (1988) concluded that the conventional broad classification of soil types is not effective for characterizing the site effects. Because site amplification factors are strongly frequency and site dependent, any averaged values for different sites with the same site category yield rather small and flat frequency characteristics, which is far from the reality at any sites in that category.

On April 29th and May 1st, 2016, we conducted microtremor measurements in the earthquake damage area of Mashiki Town, where many wooden houses were damaged. Single-station measurements of microtremors were done by using portable instruments (Figure 1-b). The clock was corrected by GPS within 1 msec. we measured microtremors along 10 observation lines from north to south, and each distance was 100-200m. we obtained microtremors records for 15-20 minutes with a sampling frequency of 100Hz at 62 sites (Figure 1-c). The interval of each sites was not even because we could not go to the several ideal points because of the house collapses.

The observed microtremors was analyzed following the standardized procedure, in which 40.96sec record sections were extracted with 50% overlapping, the Fourier spectrum of each section was earned with the 0.1 Hz Parzen window for smoothing. After working out the horizontal-to-vertical spectral

ratios of each segment, we removed the noise HVRs which were very different from other spectra. Finally, we averaged the available MHVRs of North-South (NS) and East-West (EW) directions. To find the first peak frequency of MHVRs, we calculated the root-mean-square (rms) of two components (NS/UD, EW/UD), as Equation (1) shows.

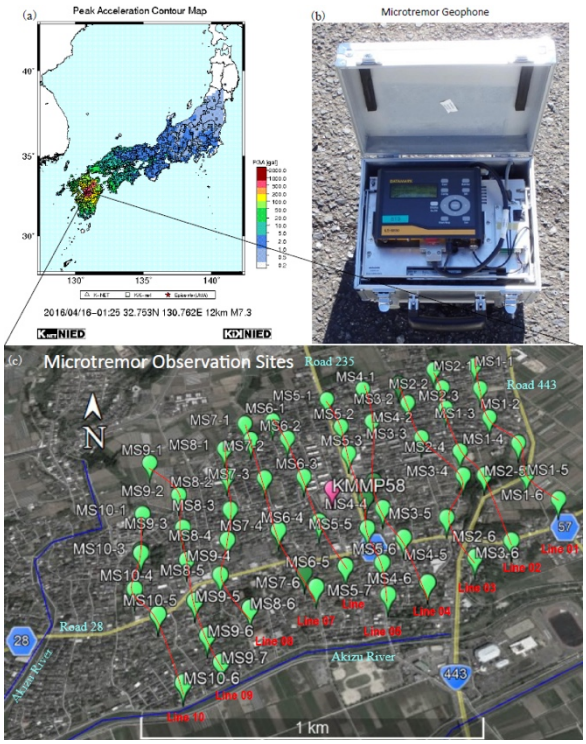

Figure 1 (a) is the PGA contour map when the mainshock occurred; (b) is the microtremor geophone which we used; (c) is the plot of the microtremor observation sites in Mashiki Town, Kumamoto city, Japan

$$MHVRs(rms) = \sqrt{\frac{[MHVRs(\frac{NS}{UD})]^2+[MHVRs(\frac{EW}{UD})]^2}{2}} \qquad (1)$$

We could find the first peak clearly on the MHVR curves of 48 sites. At Most of the sites the peak frequencies of EW and NS are nearly the same or not different so much, so we picked the peak frequency from the RMS curves. Basing on these results, we made a distribution map of predominant frequencies in Mashiki Town (Figure 2). The peak frequencies of the MHVRs are distributed in the wide range of 0.8-5.3 Hz, but most of them (88%) are in the range of 0.8-3 Hz. At only 6 sites the peak frequencies are larger than 3 Hz, and all of these 6 sites are located at eastern side of our observation area.

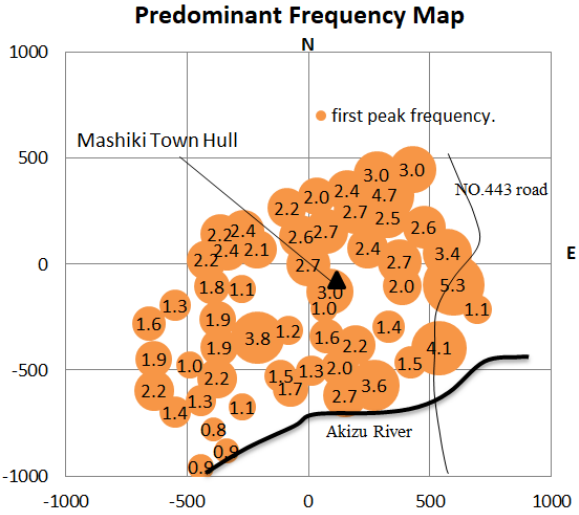

Figure 2 Predominant frequency map of Mashiki Town. The black triangle is the location of Mashiki town hall. Centers of all the orange circles are microtremor observation sites

Since the predominant frequency ranges from 1 to 5 Hz, the thickness of sediments in Mashiki town should vary from one to five times if the predominant frequencies are generated from the same layer boundary. Such a large difference in the properties should be reflected in the amplification factor and in the damage distribution. The predominant frequencies in northeastern part are larger than the ones in southwestern part, where is a flat area near the Akizu river.

3. Pseudo Earthquake Horizontal-to-Vertical Spectra Ratios

Kawase et al. (2018) proposed EHVR-to-MHVR method (EMR) to transform MHVR into pseudo-EHVR. They compared MHVR and EHVR at about one hundred K-NET and KiK-net stations in Japan. they found that MHVRs and EHVRs shared similarities, especially until the first peak frequency, but they have significant differences in the higher frequency range. It is because microtremors mainly consist of surface waves so that peaks associated with higher modes would not be prominent, while seismic motions mainly consist of upwardly propagating plain body waves, which means higher mode resonances can be seen in high frequency. They defined the ratio between EHVR and MHVR as EMR. they classified EMR into five categories based on the fundamental frequency of MHVR (peak_F), which are 0.2-1.0 Hz,

1.0-2.0 Hz, 2.0-5.0 Hz, 5.0-10.0 Hz, and 10-20 Hz. Then they took the average of the EMR normalized by peak_F in each category (Figure 3).

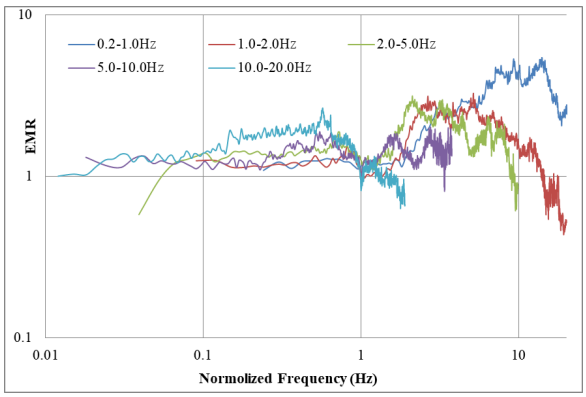

Figure 3 The normalized EMR. Peak frequency exists in 0.1–1.0 Hz (dark red); 1.0–2.0 Hz (brown), 2.02–5.0 Hz (blue), 5.02–10.0 Hz (green), 10.02–20.0 Hz (water blue)

$$pEHVR = MHVR * EMR \quad (2)$$

In this research, we used the MHVR data between 0.3-20Hz. At first, we found peak_F at frequency range of 0.3-20Hz because the peak_F of our analyzed MHVRs appeared in this range and decided the category of EMR according to the peak_F. Then the normalized frequencies of EMR were multiplied by peak_F to adjust to the frequency of MHVR. Finally, we got pEHVR by Equation (2).

We also used the strong ground motions recorded at KMMH16 and KMMP58. We chose strong ground motions with peak ground acceleration (PGA) between 1.0-50.0gal, because S-wave may not be clear if PGA is less than 1.0gal and earthquake records exceeding 50.0 gal may show the nonlinear behavior of the underground structure (Kawase et al, 2011). We used the earthquake motions recorded three months after the mainshock (after July 17th, 2016). We obtained 88 earthquake waves at KMMH16 and 90 earthquake waves atKMMP58. We calculated EHVR of EW and NS directions and we got their RMS. Then we took the average EHVR. Now, we got the EHVR at KMMH16 and KMMP58, besides we have the pEHVR and MHVR which were recorded near the KMMH16 and KMMP58 stations. We compared these MHVR, pEHVR and EHVR together and we found pEHVR is more similar to EHVR than MHVR. We would continue our research based on the pEHVR in this research. Figure 4 showed comparison of 48 pEHVR and 2 EHVR in Mashiki town.

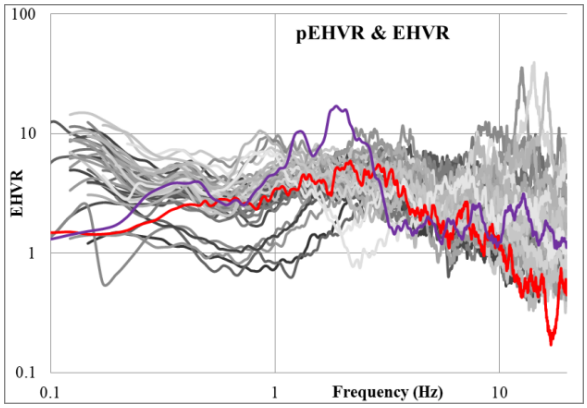

Figure 4 Comparison of pEHVR at 48 microtremors observation sites and 2 observed EHVR between 0.1-20Hz. The purple line is EHVR of KMMP58. The red line is EHVR of KMMH16

4. Shallow Subsurface Structure Identification

Table 1 Boring hole data of KMMH16

No	Thickness	Depth	Vp	Vs	Soil material
	(m)	(m)	(m/s)	(m/s)	
1	3.00	3.00	240.00	110	Clay
2	12.00	15.00	380.00	240	Sand
3	18.00	33.00	1180.00	500	Soft rock
4	8.00	41.00	1180.00	400	Sand and gravel
5	28.00	69.00	1950.00	760	
6	32.00	101.00	2300.00	820	rock
7	32.00	133.00	2800.00	1470	
8	10.00	143.00	2800.00	700	
9	26.00	169.00	2800.00	1380	
10	32.00	201.00	2300.00	840	
11	33.00	234.00	2300.00	1470	

In this research, we made two steps to identify Vs structures of observation sites. First, we made the 1st initial model reference to the borehole data (Table 1) (NIED, 2016) and J-SHIS data (Table 2) (NIED, 2018). we identified Vs and Vp by Hybrid Heuristic Searching method (Nagashima et al., 2014) and we didn't set any restraint of both of them. we set the damping as 1.1%. And the density of each layer was converted from Vs according to Equation (3).

Table 2 J-SHIS model of Mashiki area

Depth(m)	Vs(m/s)	Vp(m/s)	density(m/s^3)
358	2100	4000	2.40
2011	3200	5500	2.65
7011	3400	6000	2.75

$$\rho = 1.4 + 0.67 \times \sqrt{\frac{V_S}{1000}} \qquad (3)$$

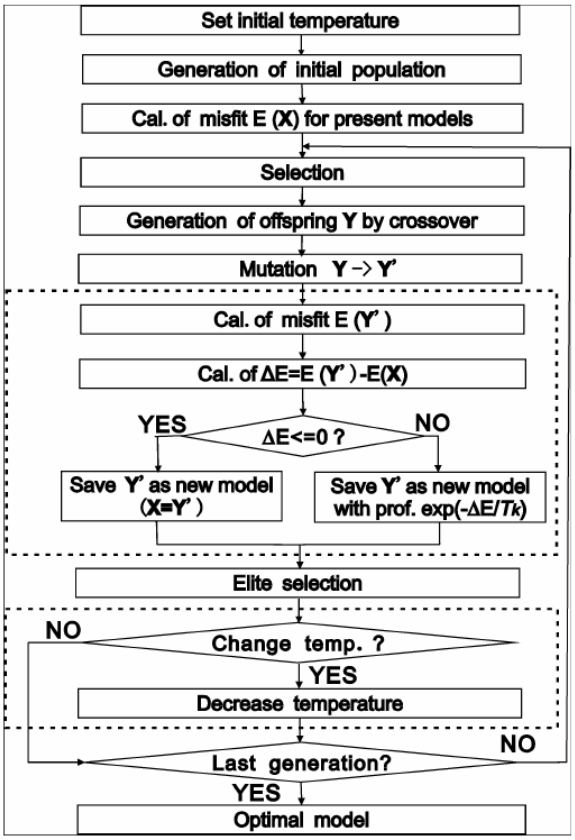

Figure 5 Calculation flow chart of the HHS method

During the calculation, the generation was 200 and the population was 400, that means we calculated 80000 times for identifying one velocity structure. We minimized the residual between pEHVR and the theoretical EHVR with the frequency range of 0.1-20Hz (but for some special sites this frequency range was different, because in the lower frequency range pEHVR and MHVR were contaminated by the noise, so we did not use such frequency range). We identified the velocity structures 10 times for one site under the same condition. After that, we chose the model whose residual was smallest among 10 trials as the best model. Finally, we got the initial model of second step by averaging all the best identified models.

Second, we set the initial model referenced to the averaged model in 1st step, while the thickness was referred the best model of each site (the lease residual case of 10 trials). Afterwards, we identified thickness again with the variation of ±80% at every site. Other parameters for identification were the same with the 1st step. The subsurface Vs structure identification process was showed in Figure 5.

We gather the identified Vs structures in Figure 6. For most sites, the depth of engineering bedrock is around 70-130m deep when Vs less than 700m/s. After estimating depth of bedrock layer (in our research, we suppose Vs of bedrock layer is larger than 3000m/s), we made the seismic bedrock layer map under Mashiki Town (Figure 7). Under Mashiki town, the seismic bedrock is usually around 1500-2000m deep. But under the northeast part, seismic bedrock is much deeper than other parts, it reaches 3500-4000m deep.

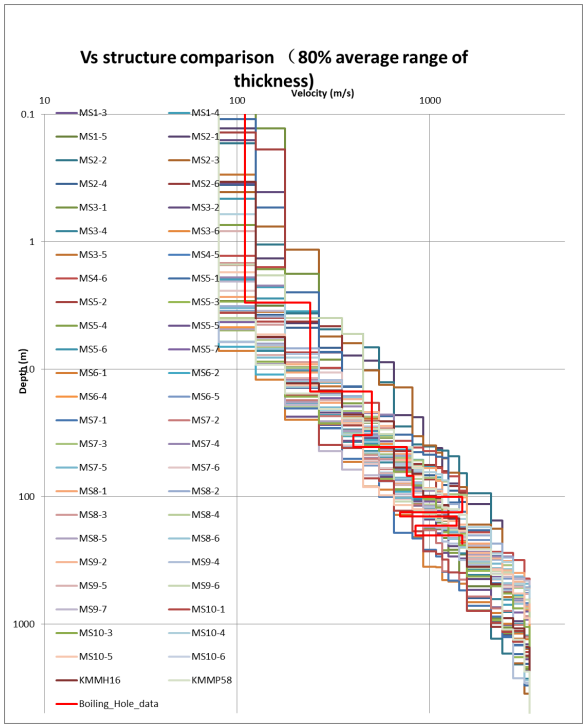

Figure 6 50 best identification Vs structure models of Mashiki town. The red line is the borehole data of KMMH16 site. Other broken lines are identification results with the smallest misfit of 10 trials of every microtremor observation site

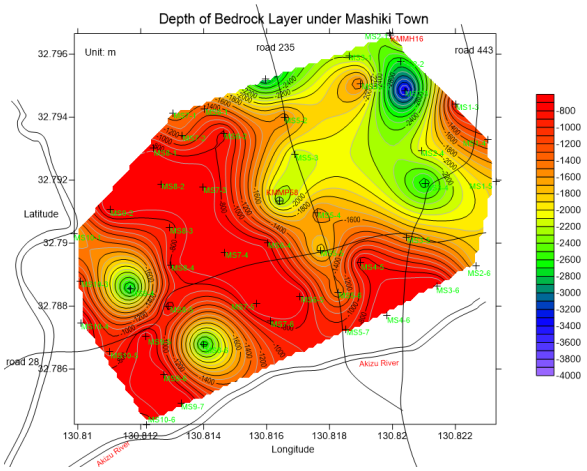

Figure 7 Estimated depth of seismic bedrock under Mashiki town

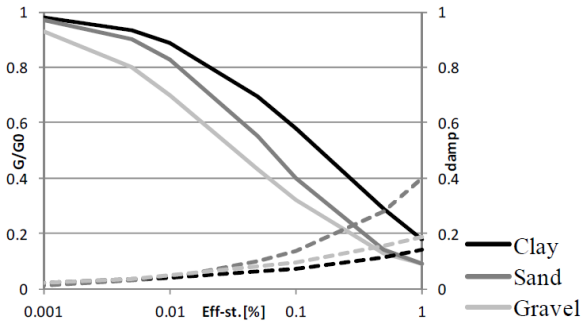

Figure 8 Properties of three kinds of soil materials, the dark solid line and dot line are shear modulus and damping of clay, the medium grey solid line and dot line are shear modulus and damping of sand, and the light grey solid line and dot line are shear modulus and damping of gravel

5. Nonlinear Site Response of the Main-Shock

As we mentioned above, there are two strong motion observation stations in Mashiki Town, Kumamoto, they are KMMH16 and KMMP58. KMMH16 is located at north of DCA (damage concentrated area) while KMMP58 is located in the center of DCA. Hiroyuki Goto et al. (2017) mentioned that, at KMMP58, 1.82m/s of PGV and 50.2m/s^2 of spectra acceleration (SA) at 1.0sec were observed, while at KMMH16 PGV and SA at 1.0sec are 1.4m/s and 23.7m/s^2, respectively.

The equivalent linear analysis (ELA) represented by SHAKE and FLUSH (Schnabel et al, 1972) is one of the most frequently used methods in the engineering practice. This method is an approximate method mainly because it uses effective strain to determine the material property for analysis. There are several reasons why equivalent linear analysis is frequently used in the engineering practice, even though they are less accurate than nonlinear methods. One of the reasons is simplicity in preparing the input data. Another reason is stability of the numerical integration. A very important advantage of the equivalent linear analysis is that the analysis can perform the deconvolution analysis by using the observed motions as the input waves when multiple reflection theory such as SHAKE is used. On the other hand, nonlinear analysis method allows only convolution analysis. Yoshida et al. (2002) propose a method to improve the equivalent linear method by expressing stiffness and damping as functions of frequency. In this part, we will use the same research method as Yoshida.

We used the nonlinear characteristics of three kinds of soil materials show in Figure 8 which was referenced to Nagashima et al (2017). To conduct ELA correctly, the selection and assignment of nonlinear characteristics are very important and delicate. We assigned the clay nonlinear characteristics to the Fill soil, Silt and Volcanic ash clay layers, the sand characteristics to Sand and the gravel characteristics to Gravel soil. By referencing to the borehole data of KMMH16, we assumed the layers with Vs between 0-176.81m/s as the clay material; the layers with Vs between 176.82-450.93m/s as sand material and the layers with Vs between 450.94-812.55m/s as gravel material; We set linear material for layers with Vs larger than 812.56m/s as rock material. Here we showed the classification standard of three kinds of soil materials based on their Vs in Table 3.

Table 3 Three kinds of soil materials: clay, sand and gravel

No	Vs (m/s)	Vp (m/s)	Soil material
1	80.12	574.26	Clay
2	124.69	751.74	
3	176.81	915.47	
4	266.01	1089.44	Sand
5	351.12	1264.4	
6	450.93	1432.77	
7	546.33	1588.06	Gravel
8	651.12	1761.67	
9	812.55	1970.11	

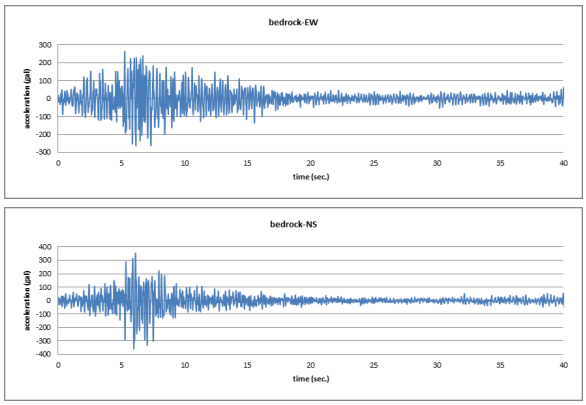

Figure 9 Estimated bedrock waves of EW and NS directions of the mainshock of the 2016 Kumamoto earthquake, the up figure is EW bedrock wave, and the down figure is NS bedrock wave

To analyze dynamic response of non-linear soil materials, we first need to get incident wave of main-shock at the seismic bedrock layer. Based on the method mentioned by Nagashima et al. (2017), we can estimate the horizontal incident spectrum at the seismic bedrock from the vertical motion observed at the surface assuming the less nonlinearity of the vertical transfer function based on diffused field theory (DFT). The main equation is as following equation:

$$spectra_{horizontal}^{bedrock} = \frac{spectra_{horizontal}^{surface}}{TF_{horizontal}} = \left(\frac{\alpha}{\beta}\right)^{1/2} * spectra_{vertical}^{surface} / TF_{vertical} \quad (4)$$

After obtaining both EW and NS incident waves at seismic bedrock layer (Figure 9), we calculated dynamic response for both linear and nonlinear cases of all the sites. We got the PGAs and PGVs at every site, and we made the distribution maps of PGV (Figure 10 and Figure 11) and PGA (Figure 12 and Figure 13) of Mashiki town.

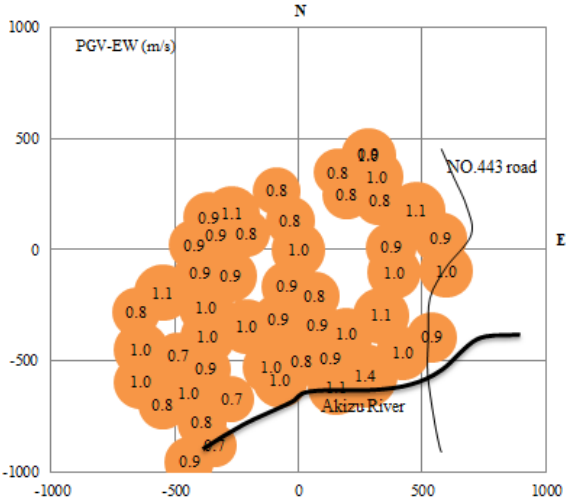

Figure 10 PGV map of EW direction during the mainshock, unit is 'm/s'. Site locations are the same as Figure 1-c. The bold dark line showed location of the Akizu river, which passes through the Mashiki town

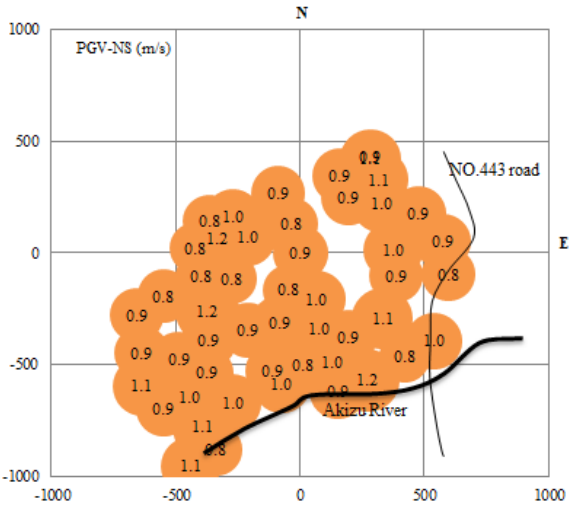

Figure 11 PGV map of NS direction during the mainshock, unit is 'm/s'. Site locations are the same as Figure 1-c. The bold dark line showed location of the Akizu river, which passes through the Mashiki town

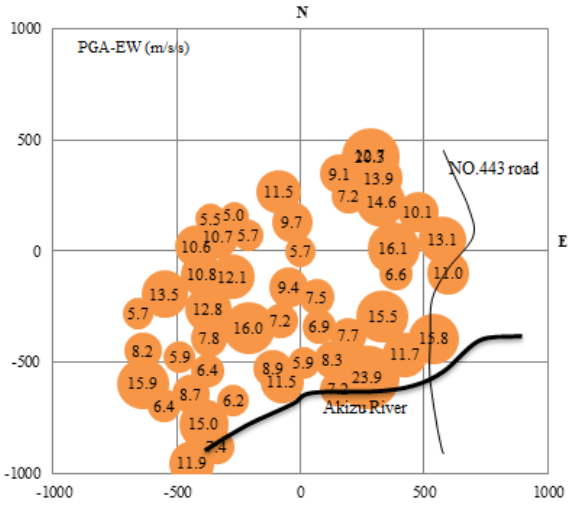

Figure 12 PGA map of EW direction during the mainshock, unit is 'm/s²'. Site locations are the same as Figure 1-c. The bold dark line showed location of the Akizu river, which passes through the Mashiki town

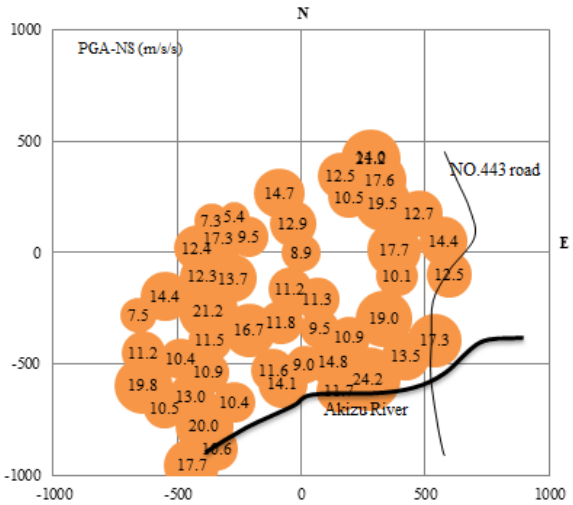

Figure 13 PGA map of NS direction during the mainshock, unit is 'm/s²'. Site locations are the same as Figure 1-c. The bold dark line showed location of the Akizu river, which passes through the Mashiki town

6. Conclusion

We observed the microtremor at Mashiki town and We made the fundamental peak frequency map of MHVR in Mashiki town. We found that the predominant frequencies of northeastern part are larger than southwestern part in Mashiki town.

We calculated pEHVR by multiplying MHVR and EMR. Comparing pEHVR and MHVR with EHVR, pEHVRs are closer to observed EHVR than MHVRs. So, we think EMR method is suitable for Mashiki Town.

We identified the subsurface structures below the microtremors observation sites by using pEHVR. The identified layers with Vs less than 700m/s were always shallower than 130m in this area. According to the seismic bedrock map, the seismic bedrock at northeastern part is deeper than other parts.

We carried out the equivalent linear analysis to obtain PGA and PGV at microtremors observation sites. As the PGVs at the sites near KMMH16 and KMMP58 sites were similar with observed PGVs at the strong motion stations. We think it is quite useful to explain the relationship between surface wave and seismic bedrock wave by Equation 4.

According to the results of linear and non-linear dynamic analysis, the estimated PGVs were about 1 m/s. We found PGV appeared stabilization while PGA were different from site to site. We think 1D subsurface structure could not explain spatial distribution of building damage. Therefore, we need to analyze site response based on 3D underground structure and estimate building damage degree distribution based on these research results.

Acknowledgement

The authors would like to thank all the members of Kawase-Nishino Labroatory, Disaster Prevention Research Institute of Kyoto University, for their great help of microtremor survey. The authors also want to thank organizations for providing strong-motions records: Kik-net which is operated by National Research Institute for Earth Science and Disaster Prevention (NIED).

References

Bard, P. (1998). Microtremor measurement: a tool for site effect estimation? In K. Irikura K. Kudo H. Okada T. Sasatami Eds (pp. 1251–1279).

Fukuyama, E., & Suzuki, W. (2016). Near-fault deformation and Dc″ during the 2016 Mw7.1 Kumamoto earthquake. Earth, Planets and Space, 68(1), 6–11.

Goda, K., Campbell, G., Hulme, L., Ismael, B., Ke, L., Marsh, R., … Wilkinson, S. (2016). The 2016 Kumamoto earthquakes: cascading geological

hazards and compounding risks. Front. Built Environ, 219(2).

Goto, H., Hata, Y., Yoshimi, M., & Yoshida, N. (2017). Nonlinear site response at KiK-net KMMH16 (Mashiki) and heavily damaged sites during the 2016 Mw7.1 kumamoto earthquake, Japan. Bulletin of the Seismological Society of America, 107(4), 1802–1816.

Kawase, H. (1996). The Cause of the Damage Belt in Kobe: "The Basin-Edge Effect," Constructive Interference of the Direct S-Wave with the Basin-Induced Diffracted/Rayleigh Waves. Seismological Research Letters, 67(5), 25–34.

Kawase, H., Matsushima, S., Nagashima, F., Baoyintu, & Nakano, K. (2017). The cause of heavy damage concentration in downtown Mashiki inferred from observed data and field survey of the 2016 Kumamoto earthquake 2016 Kumamoto earthquake sequence and its impact on earthquake. Earth, Planets and Space, 69(1), 1–11.

Kawase, H., Mori, Y., & Nagashima, F. (2018). Difference of horizontal-to-vertical spectral ratios of observed earthquakes and microtremors and its application to S-wave velocity inversion based on the diffuse field concept. Earth, Planets and Space (Vol. 70). Springer Berlin Heidelberg.

Kawase, H., Sánchez-Sesma, F. J., & Matsushima, S. (2011). The optimal use of horizontal-to-vertical spectral ratios of earthquake motions for velocity inversions based on diffuse-field theory for plane waves. Bulletin of the Seismological Society of America, 101(5), 2001–2014.

Nagashima, F., Matsushima, S., Kawase, H., Sánchez-Sesma, F. J., Hayakawa, T., Satoh, T., & Oshima, M. (2014). Application of horizontal-to-vertical spectral ratios of earthquake ground motions to identify subsurface structures at and around the K-NET site in Tohoku, Japan. Bulletin of the Seismological Society of America, 104(5), 2288–2302.

Nagashima, F., Kawase, H., & Matsushima, S. (2017). Estimation of Horizontal Seismic Bedrock Motion From Vertical Surface Motion Based On Horizontal-to-Vertical Spectral Ratios Of Earthquake Motions. Santiago, Chile: The 16th World Conference on Earthquake.

Nakamura, Y. (1989). A method for dynamic characteristics of estimation of subsurface using microtremor on the ground. Quarterly Report of RTRI.

National Institute for Land and Infrastructure Management (NILIM). (2016). Report of Committee for Causal Analysis of Building Damages during the 2016 Kumamoto Earthquake (Japanese).

Nozomu, Y. (2014). DYNEQ, A computer program for DYNamic response analysis of lever ground by EQuivalent linear method.

Nozomu, Y., Satoshi, K., & Iwao, S. (2002). Equivalent linear method considering frequency dependent characteristics of stiffness and damping. Soil Dynamics and Earthquake Engineering, 205-222.

Sánchez-Sesma, F. J., Rodríguez, M., Iturrarán-Viveros, U., Luzón, F., Campillo, M., Margerin, L., … Rodríguez-Castellanos, A. (2011). A theory for microtremor H/V spectral ratio: Application for a layered medium. Geophysical Journal International, 186(1), 221–225.

Schnabel, P., Lysmer, J., & Seed, H. (1972). SHAKE: a computer program for earthquake response analysis of horizontally layered sites. Berkeley: University of California, Berkeley.

NIED. (2016, 04). Final Report of the 2016 Kumamoto Earthquake Mainshock, From http://www.j-risq.bosai.go.jp/report/static/R/20160416012514/0424/00002/R-20160416012514-0424-00002-REPORT.html.

NIED. (2018). Japan Seismic Hazard Informatino Station. Retrieved 2017, from http://www.j-shis.bosai.go.jp/map/JSHIS2/download.html?lang=en.

Yamada, M., Ohmura, J., & Goto, H. (2017). Wooden Building Damage Analysis in Mashiki Town for the 2016 Kumamoto Earthquakes on April 14 and 16. Earthquake Spectra, 33(4), 1555–1572.

Yoshiya, H., Hiroyuki, G., & Masayuki, Y. (2016). Preliminary Analysis of Strong Ground Motions in the Heavily Damaged Zone in Mashiki Town, Kumamoto, Japan, during the Mainshock of the 2016 Kumamoto Earthquake (Mw 7.0) Observed by a Dense Seismic Array. Seismological Research Letters.

(Received Jun 13, 2018)